A&A 396, 673–682 (2002)
DOI: 10.1051/0004-6361:20021413

Astronomy & Astrophysics

Band-splitting of coronal and interplanetary type II bursts

II. Coronal magnetic field and Alfvén velocity

B. Vršnak[1], J. Magdalenić[1,2], H. Aurass[3], and G. Mann[3]

[1] Hvar Observatory, Faculty of Geodesy, Kačićeva 26, 10000 Zagreb, Croatia
[2] INAF 8211, Osservatorio Astronomico di Trieste, Via G. B. Tiepolo 11, 34131 Trieste, Italy
[3] Astrophysikalisches Institut Potsdam, An der Sternwarte 16, 14482 Potsdam, Germany

Received 5 August 2002 / Accepted 20 September 2002

Abstract. Type II radio bursts recorded in the metric wavelength range are excited by MHD shocks traveling through the solar corona. They often expose the fundamental and harmonic emission band, both frequently being split in two parallel lanes that show a similar frequency drift and intensity behaviour. Our previous paper showed that band-splitting of such characteristics is a consequence of the plasma emission from the upstream and downstream shock regions. Consequently, the split can be used to evaluate the density jump at the shock front and to estimate the shock Mach number, which in combination with the shock speed inferred from the frequency drift provides an estimate of the Alfvén velocity and the magnetic field in the ambient plasma. In this paper such a procedure is applied to 18 metric type II bursts with the fundamental band starting frequencies up to 270 MHz. The obtained values show a minimum of the Alfvén velocity at the heliocentric distance $R \approx 2$ amounting to $v_A \approx 400$–500 km s^{-1}. It then increases achieving a local maximum of $v_A \approx 450$–700 km s^{-1} at $R \approx 2.5$. The implications regarding the process of formation and decay of MHD shocks in the corona are discussed. The coronal magnetic field in the range $1.3 < R < 3$ decreases as R^{-3} to R^{-4}, or $H^{-1.5}$ to H^{-2} if expressed as a function of the height. The results are compared with other estimates of the coronal magnetic field in the range $1 < R < 10$. Combined data show that below $H < 0.3$ the magnetic field is dominated by active region fields, whereas above $H = 1$ it becomes radial, behaving roughly as $B = 2 \times R^{-2}$ with a plausible value of $B \approx 5$ nT at 1 a.u.

Key words. Sun: radio radiation – MHD – shock waves – Sun: corona

1. Introduction

The magnetic field strength, Alfvén velocity, and the plasma-to-magnetic pressure ratio β are parameters that are essential for the comprehension of processes taking place in the solar corona. Unfortunately, a direct measurement of the magnetic field in a hot low-density coronal plasma by means of the Zeeman or Hanle effect is obstructed by many difficulties (for a brief survey see Lin et al. 2000). Although a big step forward was achieved recently (Lin et al. 2000) the measurements are still burdened by a low signal-to-noise ratio, low temporal and spatial resolution and can be performed only at low heights.

Most of the information about the coronal magnetic field strength is obtained by indirect methods, generally based on two different approaches: the coronal field can be inferred by extrapolating the measured photospheric field, or by analyzing various forms of coronal radio emission (for a review see, e.g., Dulk & McLean 1978; Krüger & Hildebrandt 1993).

In this paper we utilize the method proposed by Smerd et al. (1974, 1975). It is based on measurements of type II radio bursts, known to be excited by the coronal MHD shock waves. Type II bursts usually show the fundamental and harmonic emission band, both frequently being split in two parallel lanes (cf. Nelson & Melrose 1985). Smerd et al. (1974) proposed that the band-split is associated with the density jump at the shock front, which provides an estimate of the shock Mach number. On the other hand, the shock velocity can be estimated from the frequency drift of the burst, and the ratio of the two parameters gives the Alfvén velocity.

Although the method is quite simple it has not really been exploited after the paper by Smerd et al. (1975). It has been applied only occasionally, often in an indirect way (see e.g., Gopalswamy et al. 1986; Mann et al. 1995; Magdalenić & Vršnak 2000; Vršnak et al. 2001a). The reason could be found in the barely justified hypothesis on which it relies. The proposed upstream/downstream interpretation apparently had serious drawbacks and some other explanations seemed to be more appropriate (for a review and discussion see Vršnak et al. 2001b; hereinafter Paper I). Eventually, the upstream/downstream interpretation was justified in Paper I analyzing type II bursts from interplanetary shocks reaching the Earth: several examples were found in which the extrapolation

Send offprint requests to: B. Vršnak,
e-mail: bvrsnak@geodet.geof.hr

of the two band split lanes were pointing to the base and the ramp of the local plasma frequency jump caused by the shock passage.

Since type II bursts are excited by MHD shock waves sweeping through the corona on a global scale they have the advantage of not being restricted to a flaring region itself. Moreover, type II bursts associated with coronal mass ejections are observed not only in the metric wavelength range, but also at much longer, decametric-kilometric (Dm-km) wavelengths (e.g., Bougeret 1985). Consequently, they can be used to infer the magnetic field and Alfvén velocity in the upper corona where no other diagnostic tool is available, as well as in the interplanetary (IP) space where the magnetic field can be determined only occasionally by in situ measurements.

Several reasons motivated us to perform an analysis similar to the one presented by Smerd et al. (1974, 1975). First, the data set used by Smerd et al. (1974, 1975) was relatively small and the procedure was not appropriate: The analysis included only 9 events with the highest observed fundamental band frequency 80 MHz, and the Mach number was evaluated using the hydrodynamic approximation ($\beta = \infty$). We have selected a two times as large a data set of 18 type II bursts embracing starting (fundamental band) frequencies up to 270 MHz, and a more detailed and more accurate analysis is performed.

A further motive was that such an analysis can resolve some open questions regarding the process of formation and evolution of coronal and IP shocks, i.e. the bias between the blast and piston formation mechanisms (see, e.g., Gopalswamy et al. 1998; Cliver et al. 1999).

Finally, the following analysis lays the ground for the proper treatment of the Dm-km type II bursts that provide information about the magnetic field in the upper corona and interplanetary space. Since the Dm-km type II shocks propagate on the solar wind environment that is considerably different from that of the corona, we delay their discussion for a separate paper.

In Sect. 2 we briefly describe the method and the approximations used. In order to make reading easy, the mathematical relations used are given in the Appendix. The observations, measurements, and procedure of data reduction are presented in Sect. 3. The results are presented and discussed in Sects. 4 and 5, respectively, and the conclusions are drawn in Sect. 6.

2. The method and assumptions

Adopting the interpretation in terms of the plasma emission from the upstream and downstream shock regions, the band-split frequencies map the electron densities behind and ahead of the shock front. In front of the shock (upstream region) the plasma is characterized by the electron density n_1 and emits radio waves at the frequency f_L (lower frequency branch; LFB). The plasma behind the shock (downstream region) is compressed to the density $n_2 > n_1$ corresponding to the frequency $f_U > f_L$ (upper frequency branch; UFB). Defining the relative band-split (Fig. 1, see also Paper I) as:

$$BDW = (f_U - f_L)/f_L \tag{1}$$

and bearing in mind $f \propto \sqrt{n}$, the density jump at the shock can be expressed as:

$$X \equiv \frac{n_2}{n_1} = \left(\frac{f_U}{f_L}\right)^2 = (BDW + 1)^2. \tag{2}$$

Once the compression X is known, the Alfvén Mach number M_A can be estimated (see Appendix). Note that in MHD shocks the condition $X < 4$ is always satisfied (cf. Priest 1982), implying $f_U/f_L < 2$ and $BDW < 1$.

On the other hand, the emission frequency f can be transformed into the radial distance r by assuming some density distribution function $n(r)$. Consequently, the shock propagation speed $v = \partial r/\partial t$ can be inferred from the frequency drift $\partial f/\partial t$, providing evaluation of the Alfvén velocity $v_A = v/M_A$. Finally, the magnetic field can be found using (m.k.s.): $B = v_A\sqrt{\mu\rho} = 0.51 \times 10^{-17} f v_A$, where the coronal plasma density is approximated as $\rho \approx m_p n$, and $\mu = 4\pi \times 10^{-7}$ H m^{-1}. A more practical expression reads:

$$B\,[\text{gauss}] = 5.1 \times 10^{-5} \times f\,[\text{MHz}] \times v_A \left[\text{km s}^{-1}\right]. \tag{3}$$

The procedure is obviously model dependent: *i*) The inferred height and the velocity of the radio source depend on the coronal density model and on the angle ϕ between the direction of the source motion and the density gradient; *ii*) The relationship between the Alfvén Mach number M_A and the density jump X is a parametric function of the plasma-to-magnetic pressure ratio β in the upstream region and the angle θ between the shock normal and the upstream magnetic field (see Appendix).

The emission frequency depends on the local electron density which can be a complicated function of space coordinates, especially in active regions. We note that most of the measurements are performed at frequencies corresponding to relatively large heights, well outside of the active region core. Therefore we assume that the plasma density depends only on the height. In particular, the Saito (1970) and Newkirk (1961) density models with various base densities are applied (see Fig. 8 in Appendix).

Radioheliographic observations indicate that the type II burst sources frequently do not propagate radially, especially at the onset of the burst (see, e.g., Nelson & Robinson 1975; Klassen et al. 1999; Klein et al. 1999). This means that the shock velocity v' is generally underestimated if the radial propagation is assumed. Accordingly, smaller values of the Alfvén speed and the magnetic field are obtained. For a given angle ϕ between the (radial) density gradient and the direction of the source motion, the true source velocity is found using $v = v'/\cos\phi$. Therefore, if ϕ = const. the evaluation of true velocity is reduced to a simple multiplication of the model densities by factor $k = \cos\phi < 1$. For example, the same speed is obtained by using the five-fold Saito density model and $\phi = 60^o$, or by applying the ten-fold Saito model and $\phi = 0^o$.

In a statistical sense the problem can be solved by introducing the mean angle $\overline{\phi}$ at which an "average source" moves through an "average corona". Assuming that most often the corona can be described by the two- to five-fold Saito model, we will present also the outcome for the ten-fold Saito model with $\overline{\phi} = 0$ to represent the propagation in the five-fold Saito

model corona under assumption of a strong, $\overline{\phi} = 60^{\rm o}$, deviation from the radial propagation.

The MHD relationship between the density jump and the Mach number depends on the angle θ between the shock normal and the magnetic field direction. In the quasi-perpendicular regime between $\theta = 90^{\rm o}$ and, say, $\theta = 60^{\rm o}$ the outcome is only weakly dependent on the value of θ (see Fig. 9a in Appendix). Comparing the longitudinal, $\theta = 0^{\rm o}$, and the perpendicular, $\theta = 90^{\rm o}$, propagation one finds that the calculated values of $M_{\rm A}$ are 10–25% lower in the longitudinal case, the difference being larger for a larger band-split.

Another important parameter is the plasma-to-magnetic pressure ratio $\beta = 2\mu p/B^2$ in the upstream region (see Fig. 9b in Appendix). Highly structured patterns observed in the EUV wavelength range indicate that the coronal plasma is controlled by the magnetic field, i.e., $\beta \ll 1$ (for a discussion see Gary 2001). Since the relationship $M_{\rm A}(BDW)$ only weakly depends on the value of β when it is smaller than $\approx$0.2 (see Fig. 9b in Appendix) we apply $\beta = 0$. This approximation will be checked finally: after the $B(r)$ dependence is established using some density model $n(r)$, the assumption $\beta = 2\mu nkT/B^2 \ll 1$ can be verified taking for the coronal temperature $T = 1\text{–}2 \times 10^6$ K (Chae et al. 2002).

In order to check how much various approximations affect the results, the analysis is carried out using several different values for all relevant parameters.

3. Measurements and raw results

In this paper we investigate 18 coronal type II bursts recorded in the decimetric-metric (dm-m) wavelength range. The basic rule in selecting the events was that they clearly show a simple band-split pattern obeying the criteria defined in Paper I. Out of the 18 chosen events, 12 events were recorded by the radio spectrograph of the *Astrophysikalisches Institut Potsdam* covering the frequency range 40–800 MHz (Mann et al. 1992) and 6 were observed by *Culgoora Solar Observatory* radio spectrograph sweeping over the frequency range 18–1800 MHz (Prestage et al. 1994; see `http://www.ips.oz.au/culgoora/spectro/index.html`). The measurements were performed at the harmonic emission band[1] since in dm-m type II bursts it is usually stronger and better defined then the fundamental band (see, e.g., Fig. 1 where a part of the fundamental band can be seen in the 50–40 MHz range around 10:00 UT). In some cases measurements of equal accuracy were possible at both emission bands, showing no significant difference in the outcome (see also Smerd et al. 1974, 1975; Mann et al. 1996).

In Fig. 1 the procedure of measurements is illustrated by showing one of the analysed type II bursts (see also Fig. 2 in Paper I). The LFB and UFB of the band-split emission are marked by the lines that follow the two emission ridges. The period of type II burst emission is divided into a number of roughly equidistant subintervals, defined by the times t_1 to t_N. At each of these N moments the frequencies of the emission maximum at LFB and UFB ($f_{\rm L}$ and $f_{\rm U}$, respectively) were measured, providing the relative band-splits $BDW(t_i)$ defined by Eq. (1).

The number of $[f_{\rm U}(t_i),\ f_{\rm L}(t_i)]$ data pairs varied from 3 to 22 per event, depending on the duration and frequency range covered by a particular type II burst. From the obtained data the frequency drifts:

$$D_f\left(\overline{t}_i\right) \equiv \left(-\frac{\partial f}{\partial t}\right)_i = \frac{f_{\rm L}(t_i) - f_{\rm L}(t_{i+1})}{t_{i+1} - t_i}, \tag{4}$$

and the relative band-splits:

$$BDW_i \equiv BDW\left(\overline{t}_i\right) = \frac{BDW(t_{i+1}) + BDW(t_i)}{2} \tag{5}$$

are determined for the depicted time intervals, where $\overline{t}_i = (t_{i+1} + t_i)/2$. These measurements are presented in Fig. 2, where the frequency drifts and band-splits are shown as a function of the LFB frequency $f_{\rm L}$.

Figure 2a shows that the frequency drift is a distinct power-law function of the frequency. In Paper I it was shown that the power-law dependence $D_f(f)$ extends to the kilometric wavelength range. The slope of $D_f(f)$ found therein for the frequency range from 10 MHz to 30 kHz is almost the same, amounting to $\approx$1.9.

Figure 2b shows no correlation between the band-split of metric type II bursts and the frequency. In the inset of Fig. 2b the distribution of values of BDW is presented showing that the majority of the analysed type II bursts has the relative band-split between 0.15 and 0.35.

4. Results

Utilizing the density models defined in Sect. 2 the frequencies $f_{\rm L}(t_i)$ are converted to radial distances $R_i(t_i)$, where $R = r/r_\odot$ is the heliocentric distance normalized with respect to the solar radius $r_\odot$. The obtained values are used to determine the radial velocities:

$$v_i\left(\overline{t}_i\right) = \frac{R(t_{i+1}) - R(t_i)}{t_{i+1} - t_i}\ r_\odot. \tag{6}$$

In Figs. 3a and b we show graphs $v_i(R_i)$ and $X_i(R_i)$, where $R_i = [R(t_{i+1}) + R(t_i)]/2$, and X_i is defined by Eqs. (2) and (5). Using the expressions given in Appendix and applying various combinations of θ and β the values $X_i(R_i)$ are converted to $M_{{\rm A}i}(R_i)$. The outcome for $\beta = 0$ and $\theta = 90^{\rm o}$ is presented in Fig. 3c. The inferred shock velocity v decreases with the heliocentric distance, whereas the values of the density jump X (and thus the inferred $M_{\rm A}$) do not show a systematic increase or decrease. Yet it should be noted that at $R \approx 2$, where the shock velocities show a local minimum, the density jumps show a local maximum.

The values $v_i(R_i)$ and $M_{{\rm A}i}(R_i)$ are used to evaluate the Alfvén velocity $v_{{\rm A}i}(R_i) = v_i/M_{{\rm A}i}$ and the corresponding magnetic field (Eq. (3)). The results are shown in Fig. 4 for the two-fold Newkirk density model so that the $B(R)$ dependence can be compared with the results reported by Smerd et al. (1974, 1975) which are shown by gray crosses in Fig. 4b.

[1] All of the harmonic frequencies were converted to the fundamental ones by halving the values.

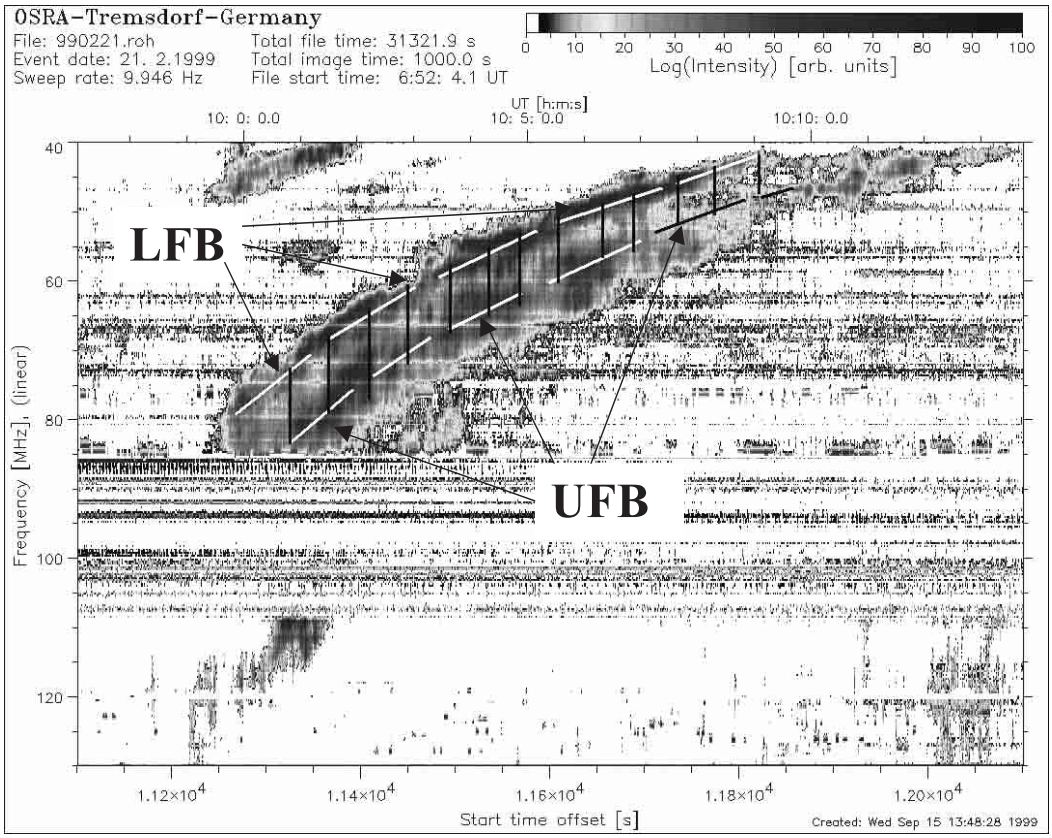

Fig. 1. Measurements of $f_U(t_i)$ and $f_L(t_i)$ at the upper and lower frequency branch (UFB and LFB, respectively) of the harmonic band in the type II burst of 21 February 1999. LFB and UFB of the band-splitting are indicated by the lines following the emission ridges and defining the frequencies f_L and f_U. Vertical lines show the times t_i at which f_L and f_U are measured.

The $v_A(R)$ dependence shows a local minimum at $R \approx 2$. It is somewhat less exposed if the Saito model is applied (the values based on the five-fold Saito model are shown in the inset of Fig. 4a) due to a less steep slope of $n(R)$ around that distance (see Fig. 8 in the Appendix). However, whatever polynomial fit is used, at least an inflection in the fitted curve is found. We note that the results do not change significantly if the two data points showing a comparatively high Alfvén velocity at $R \approx 1.3$ are removed.

In Figs. 5 and 6 the average values $\overline{v}_A(\overline{R})$ and $\overline{B}(\overline{R})$ are shown, where each data point represents the mean of 40 distance-successive data points. This representation is chosen to illustrate more transparently how different choices of β (Figs. 5a and 6a), propagation angle θ (Figs. 5b and 6b), and a density model (Figs. 5c and 6c) affect the results. Clearly, the results are most sensitive on the choice of the density model. Figure 5 indicates again that there is a local minimum, or at least a stagnation in the decrease of v_A at $R \approx 2 \pm 0.3$.

The $B(R)$ dependence can be approximated well by the power law fit of the form $B(R) = aR^{-b}$. The results are summarized in Table 1 where the power-law coefficients a and b are given. In Table 1 we also show the coefficients for the power-law fit expressing the magnetic field as a function of the normalized height $H \equiv R - 1$. Inspecting Table 1 one finds that the Saito model gives somewhat steeper decrease of the magnetic field with the distance than the Newkirk model. If the magnetic field decrease is expressed as a function of the height above the solar surface, the slope is in the range $b \approx 1.5$–2, where the former value corresponds to the two-fold Newkirk model. Similar results are obtained if the averaged data shown in Fig. 6 are used, now with the correlation coefficients $C > 0.98$.

5. Discussion

5.1. Starting assumptions

Figures 5 and 6 show that the inferred values of the Alfvén velocity and magnetic field do not significantly depend on the choice of the plasma parameter β and the propagation angle θ. Comparing Figs. 5a and 5b with Fig 4a, as well as Figs. 6a and 6b with Fig. 4b, one finds that the effect is much smaller than the data scatter.

The thick gray curve in Fig. 4b represents the magnetic field $B^* = 2\mu nkT/\beta^*$ defined by the two-fold Newkirk density model, the temperature $T = 1.5 \times 10^6$ K, and $\beta^* = 1$. Only ten data points fall below the curve, i.e. into the $\beta^* > 1$ region. Note that these data points are well isolated from the rest of the sample and could be treated as exceptions. In the case of the five-fold Saito model only five data points show $\beta^* > 1$.

The magnetic field $B^*(R)$ defined by the five-fold Saito density model, the temperature $T = 2 \times 10^6$ K, and three values of β^* (1, 0.1, and 0.01) is compared with the measurements in Fig. 6a. The measured values $\overline{B}(\overline{R})$ match closely the curve

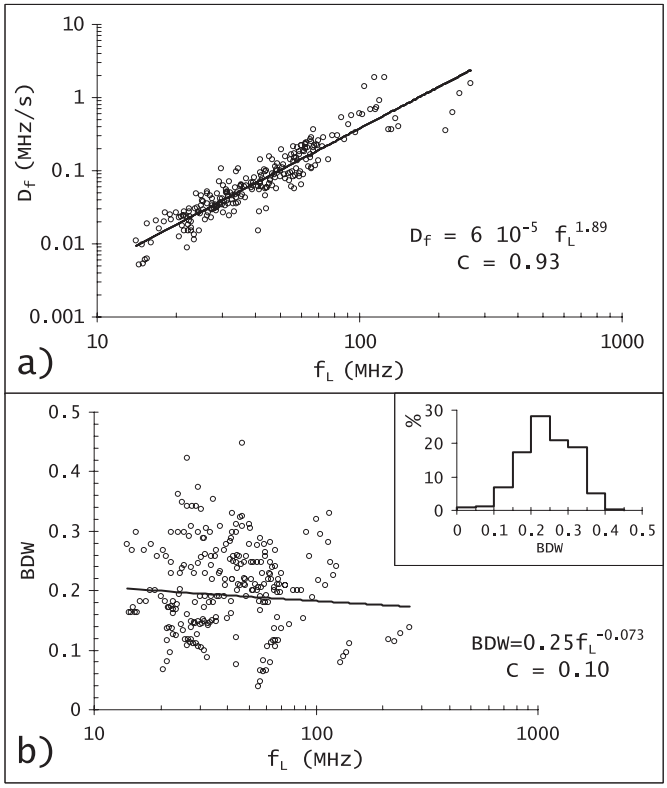

Fig. 2. Measured values of **a)** frequency drift and **b)** band-split, presented as a function of the (fundamental) frequency at LFB, f_L. The power-law least squares fits and the corresponding correlation coefficients C are shown. The histogram in the inset in the lower panel shows the distribution of relative band-splits. The presented data are based on the measurements of 18 type II bursts.

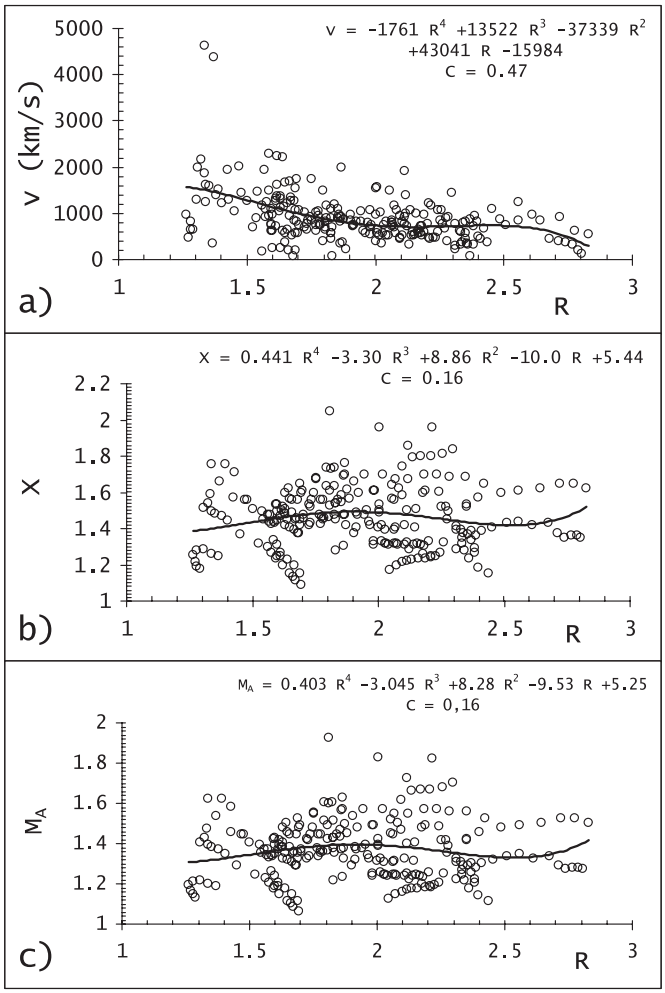

Fig. 3. Results obtained applying the five-fold Saito density model: **a)** shock velocities; **b)** downstream/upstream density jump; **c)** Alfvén Mach number obtained using $\beta = 0$ and assuming the perpendicular propagation ($\theta = 90^o$). The 4th degree polynomial least square fits are shown.

Table 1. Power-law coefficients a and b and correlation coefficients C for the $B(R)$ and $B(H)$ dependence.

model	$B(R) = aR^{-b}$			$B(H) = aH^{-b}$		
	a	b	C	a	b	C
2×Saito	7.9	4.44	0.82	0.41	1.49	0.81
5×Saito	17.6	4.22	0.83	0.89	1.85	0.83
10×Saito	29.2	3.94	0.82	1.77	2.00	0.83
2×Newkirk	9.6	3.40	0.76	0.86	1.50	0.78

$B^*(R)$ defined by $\beta^* \approx 0.1$. This justifies the applied approximation $\beta = 0$ since the difference in the results obtained by taking $\beta = 0.1$ and $\beta = 0$ is negligible. We note that the slope of $\overline{B}(\overline{R})$ is steeper than $B^*(R)$ which is consistent with the expected increase of the parameter β with the height (see, e.g., Gary 2001 and references therein).

Figures 5b and 6b show that the variation of the propagation angle θ affects the results even less than the choice of β. Inspecting Fig. 9a one finds that at $BDW = 0.35$ the difference in M_A for $\theta = 90^o$ and $\theta = 0^o$ amounts to ≈20%. Since only 2% of events are characterized by $BDW > 0.35$ the average values of v_A and B are not significantly influenced by different choices of θ.

Figures 5 and 6 show that the inferred values of the Alfvén velocity and the magnetic field are most sensitive on the density model used. When applying a higher density model, the values of v_A and B become larger. At the same time the corresponding radial distances increase. The slopes of $v_A(R)$ and $B(R)$ relationships at a given R depend directly on the slope of $n(R)$ which is different in each model (see Fig. 8 in the Appendix).

The ambiguity in choosing the density model results in a range of possible values of Alfvén velocity. For example, presuming that two- to ten-fold Saito model embraces most of the situations involved (see Sect. 2), one finds that at $R \approx 1.6$ the Alfvén velocity spans between 450 and 1300 km s^{-1}. The corresponding magnetic field is in the range 1–7 G.

Such a span of $\overline{B}(\overline{R})$ values is comparable with the scatter of individual data points. This can be seen in Fig. 4b where the two thin lines that represent $\overline{B}(\overline{R})$ values obtained by using two- and ten-fold Saito model embrace a large majority of the data points. Since the data scatter is much larger than the errors of measurements, the scatter has to be attributed primarily to the diversity of the coronal conditions and to different angles between the direction of the shock propagation and the density gradient.

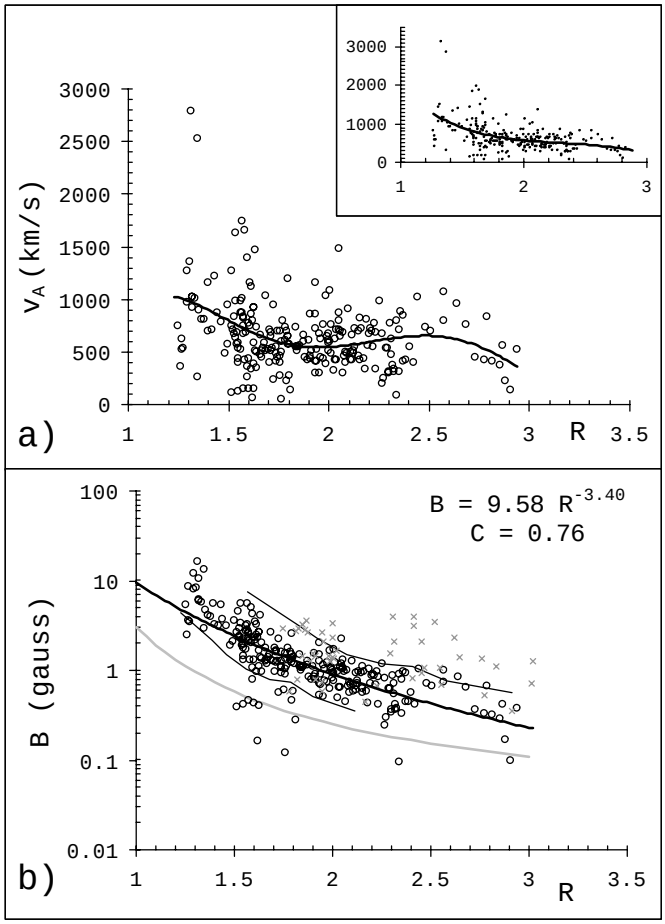

Fig. 4. a) Alfvén velocity and **b)** magnetic field, evaluated assuming the perpendicular shock propagation ($\theta = 90^{\rm o}$), the two-fold Newkirk coronal density model, and $\beta = 0$. The 5th degree polynomial least squares fit is presented for $v_{\rm A}(R)$. Note the local minimum at $R \approx 2$ and maximum at $R \approx 2.5$. In the inset the $v_{\rm A}(R)$ graph is shown for the five-fold Saito density model, showing somewhat less pronounced minimum and maximum of $v_{\rm A}(R)$ than in the two-fold Newkirk model results. In the bottom graph the power-law fit is presented (bold). The two thin lines represent the mean values shown in Fig. 6c for the two- and ten-fold Saito model. The gray curve represents values of B^* defined by two-fold Newkirk model, $T = 1.5 \times 10^6$ K, and $\beta^* = 1$. The results by Smerd et al. (1974, 1975) are shown by gray crosses.

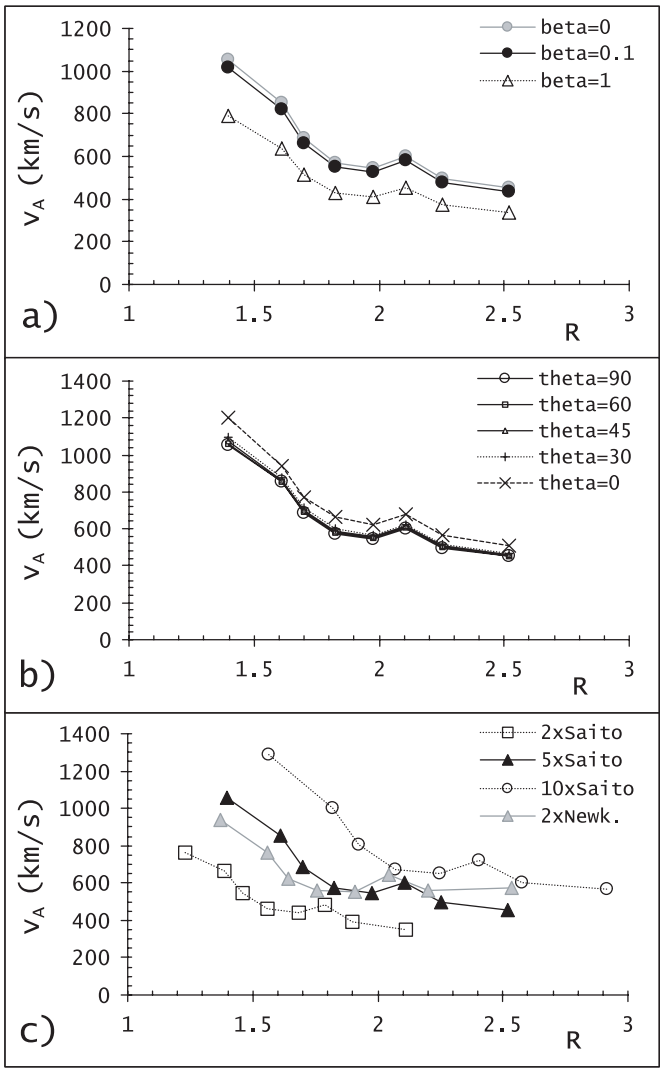

Fig. 5. Alfvén velocity shown as a function of heliocentric distance for: **a)** five-fold Saito coronal density model and $\theta = 90^{\rm o}$, with: $\beta = 0$ (gray circles), $\beta = 0.1$ (black circles), and $\beta = 1$ (triangles); **b)** five-fold Saito density model and $\beta = 0$, with: $\theta = 90^{\rm o}$ (perpendicular shock), $\theta = 60^{\rm o}$, $\theta = 45^{\rm o}$, $\theta = 30^{\rm o}$, and $\theta = 0^{\rm o}$ (longitudinal shock) **c)** $\beta = 0$, $\theta = 90^{\rm o}$, for: two-, five-, and ten-fold Saito density model, as well as two-fold Newkirk model (drawn by squares, black triangles, circles, and gray triangles, respectively.)

Finally it should be noted that the magnetic field strengths obtained by Smerd et al. (1974, 1975) are about two times larger than found herein (Fig. 4b). We emphasize that this cannot be explained by the hydrodynamic approximation ($\beta = \infty$) used therein, since the corresponding difference would not be larger than 10–20% for the considered range of values of BDW (see Fig. 9b in Appendix). Unfortunately in Smerd et al. (1974, 1975) the procedure of measurement is not described in detail, so we cannot resolve the origin of this discrepancy.

5.2. Radial dependence of the magnetic field

The range of magnetic field strengths exposed in Fig. 6c is generally consistent with the values often found at these heights (cf. Dulk & McLean 1978; Krüger & Hildebrandt 1993). In Fig. 7 our results, represented by the shaded gray area that covers the range of values defined by Fig. 6c, are exposed in a wider context. A number of estimates based on different methods are shown, mostly reported after the paper by Dulk & McLean (1978). The data are clearly clustered along the $B(H) = 5\ H^{-1.5}$ relationship proposed by Dulk & McLean (1978) for $1 < R < 10$ (thick gray line in Fig 7).

If particularly the $B(H)$ dependence found from our measurements is considered, it shows a slope between $H^{-1.5}$ and H^{-2}, the former value being obtained by using the Newkirk density model. The result can be considered as compatible with the Dulk & McLean (1978) relationship since our measurements cover only the $1.3 < R < 2.9$ range.

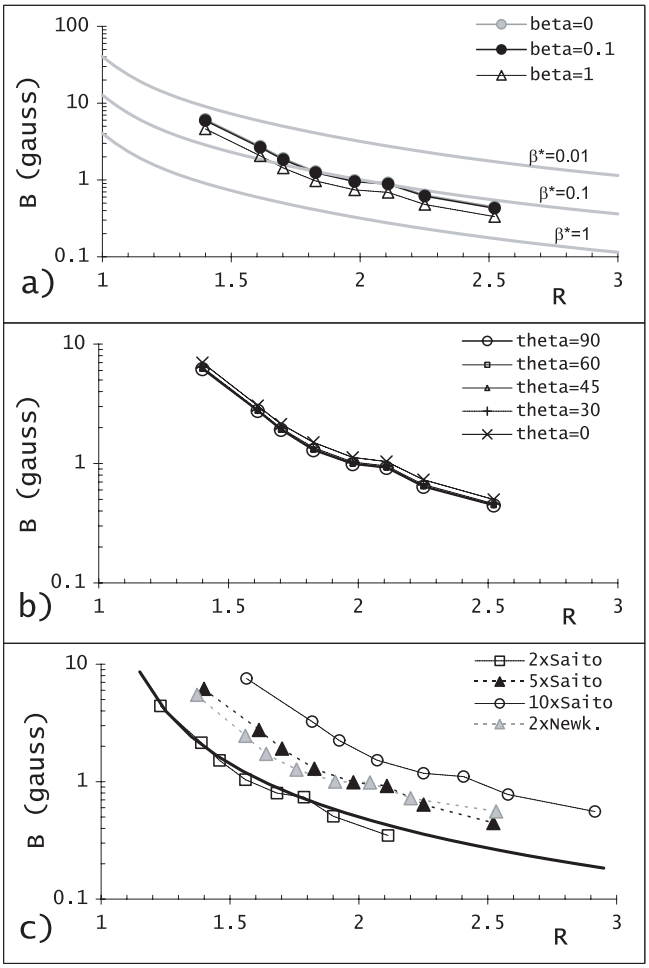

Fig. 6. Magnetic field shown as a function of heliocentric distance for the same combinations of parameters as used in Fig. 5. The $\beta = 0$–0.1 and $\theta = 30^{\rm o}$–$90^{\rm o}$ curves are not resolved (the top and middle panel, respectively). In the top panel the curves $B^*(R)$ defined by the five-fold Saito model and $T = 2 \times 10^6$ K are drawn for $\beta^* = 0.01$, $\beta^* = 0.1$, and $\beta^* = 1$ by thick gray lines. In the bottom panel the relationship $B = 0.5\ H^{-1.5}$ proposed by Dulk & McLean (1978) is shown by the bold line.

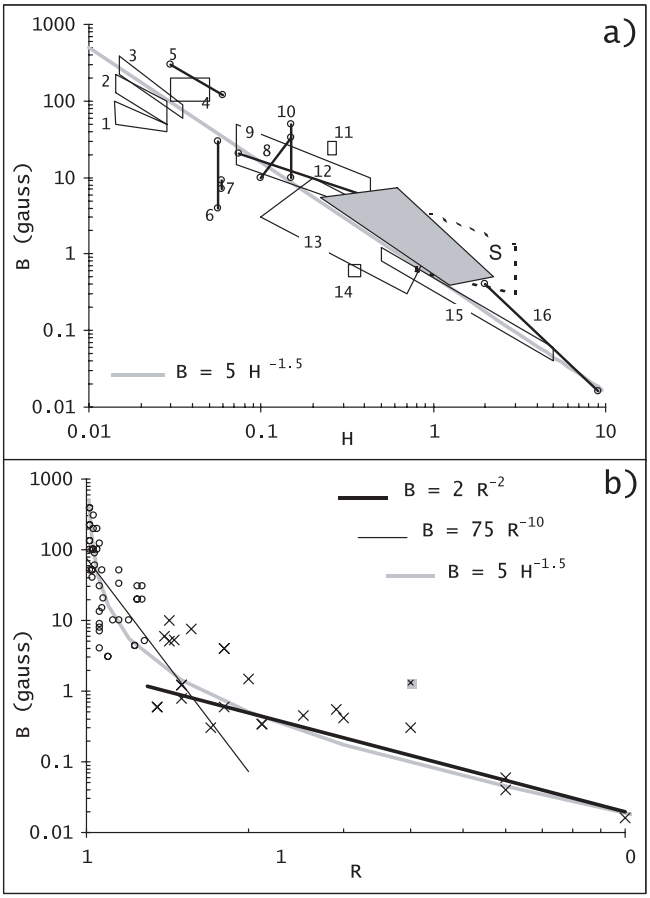

Fig. 7. a) Comparison of our results (shaded area covers the results based on two- to ten-fold Saito density model) with some other estimates: 1-3 – Brosius et al. (1993, 1997); 4 – Ramaty & Petrosian (1972); 5 – Kakinuma & Swarup (1962); 6 – Nakariakov & Ofman (2001); 7 – Aurass et al. (1987); 8 – Lin et al. (2000); 9 – Bogod et al. (1993); 10 – Ledenev et al. (2002); 11 – Yu & Yao (2002); 12 – Mann & Baumgärtl (1988); 13 – Gopalswamy et al. (1986); 14 – Mollowo (1988); 15 – Dulk et al. (1976); 16 – Patzold et al. (1987). The results obtained by Smerd et al. (1974, 1975) are framed by dashed line and denoted by S. **b)** The same data (limiting values) presented in the $B(R)$ graph, provisionally divided into two groups showing different slopes ($R < 1.3$ – circles, $R > 1.3$ – crosses). The bold and thin lines show $B = 2 \times R^{-2}$ and $B = 75 \times R^{-10}$, respectively.

As already noted by Dulk & McLean (1978) the $B(H) \propto H^{-1.5}$ relationship, except at low heights, behaves similar to the R^{-2} curve, revealing a dominance of the radial field. In Fig. 7b we represent the data from Fig. 7a in the $B(R)$ graph, splitting the sample into the $H > 0.3$ and $H < 0.3$ data sets. Each data point represents the limiting values of different estimates shown in Fig. 7a. The $B(H) = 5\ H^{-1.5}$ relationship is drawn by thick gray line. The other two lines show the functions $B = 75 \times R^{-10}$ and $B = 2 \times R^{-2}$ (thin and bold, respectively). The former relationship matches roughly the data below $R < 1.3$. The second one is chosen since at 1 AU it gives $B \approx 5$ nT, i.e. the value usually measured at the Earth. The $R > 1.3$ data show a lower limit lying closely by the R^{-2} curve. Except the shaded data point, representing the upper-right corner of the "S"-box in Fig. 7a (the data by Smerd et al. 1974, 1975), the upper boundary also approaches the R^{-2} curve beyond $R \approx 2$. This indicates that the magnetic field is dominated by active region fields below $H \approx 0.3$ and the radial field above $H = 1$. Such a result is consistent with the polarimetric measurements in the Fe XIII 10747 Å line reported recently by Habbal et al. (2001).

5.3. Radial dependence of the Alfvén speed

The dependence of the Alfvén velocity on the height does not depend qualitatively on the density model used (Fig. 5b). For the two- to ten-fold Saito model the Alfvén velocity shows a local minimum of $v_{\rm A} \approx 400$–500 km s^{-1} at $H \approx 0.7$–1.2, and a maximum of $v_{\rm A} \approx 450$–700 km s^{-1} at $H \approx 0.8$–1.5.[2]

[2] Assuming that the decrease of Alfvén velocity is monotonic, one has to assume, e.g., that below $R \approx 1.7$ the five-fold Saito model should be applied whereas above this height the two-fold Saito model should be adopted.

Such a behaviour of the Alfvén speed was anticipated by Mann et al. (1999, 2002): outside of active regions, where the radial magnetic field dominates v_A should attain maximum at the height of 2–3 solar radii (Mann et al. 1999); If the bipolar magnetic field of an active region is added, a local minimum appears between the solar surface and the region of the Alfvén velocity maximum (Mann et al. 2002).

Our results find the minimum at somewhat larger height than calculated by Mann et al. (2002), whereas the maximum is for about 1 solar radius lower. Nevertheless the qualitative behaviour is the same, bearing in mind that we have a comparatively small number of data points at $R > 2.5$ (Fig. 4a) so the height of the maximum is ambiguous.

The described height dependence of the Alfvén velocity is important for the comprehension of the formation and evolution of MHD shocks in the solar corona. Vršnak & Lulić (2000) analysed steepening of the large amplitude perturbation (simple wave) into the shock in the uniform Alfvén velocity environment. The frontal part of the perturbation is steepening because later segments (having larger amplitude) are faster than the earlier ones. The effect is obviously enhanced if the Alfvén velocity decreases in the direction of the propagation of the disturbance. Thus, the shock formation is expected to occur in the $R < 2$ range where the Alfvén speed decreases. This is compatible with typical type II burst starting frequencies of ≈100 MHz (cf. Nelson & Melrose 1985). Analogously, the shock weakens in the opposite situation. In an environment characterized by increasing Alfvén velocity the amplitude of the shock decreases and eventually becomes too weak to generate the type II burst emission. This is most likely to happen in the region before the v_A maximum, i.e. around $R \approx 2.5$, compatible with the usual dm-m type II burst ending frequencies of about 20 MHz (cf. Nelson & Melrose 1985).

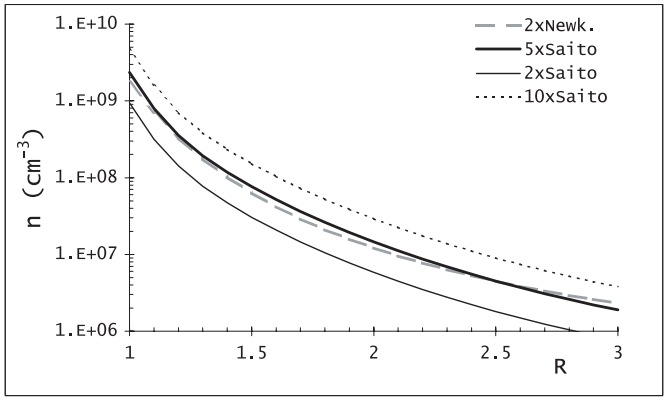

Fig. 8. The coronal density models used.

6. Conclusions

The applied method provides plausible values for the coronal Alfvén velocity and magnetic field. The data scatter is much larger than the errors of measurement thus indicating a diversity of densities and field strengths in the corona. The magnetic field strength decreases from 1–7 G at $R \approx 1.6$ to 0.3–0.9 G at $R \approx 2.5$. Such a result is in a good agreement with other estimates at this height range, as well as with the $B = 5H^{-1.5}$ relationship proposed by Dulk & McLean (1978). When placed in the wider context together with the data covering the $1 < R < 10$ range, the data indicate that below the height of $H \approx 0.3$ the magnetic field is governed by the active region fields. Above $H \approx 1$ the radial field, decreasing as R^{-2}, becomes dominant.

The results show that the coronal value of the parameter β is around $\beta \approx 0.1$, slowly increasing with the height. This is consistent with the generally decreasing trend of the Alfvén velocity (Fig. 3a) since the coronal temperature can be considered as approximately constant. Beside the overall decreasing trend, the data indicate that there is a local minimum of the Alfvén velocity of $v_A \approx 400$–500 km s^{-1} at $R \approx 1.7$–2.2 and a local maximum of $v_A \approx 450$–700 km s^{-1} at $R \approx 1.8$–2.5, depending on the coronal density model used. Such behaviour of the Alfvén velocity is qualitatively similar to that anticipated by Mann et al. (2002).

The inferred shock velocities decrease, whereas the density jumps increase in the region of $v_A = \min$. Most of the dm-m type II bursts start at heights lower or close to the Alfvén velocity minimum and cease close to the heights where it attains the maximum.

Finally, we note that the frequency drift of dm-m type II bursts depends on the emission frequency as a power-law $D_f \propto f_L^{1.9}$, very similar to that found by Vršnak et al. (2001b) in IP type II bursts.

Acknowledgements. We are grateful to the Culgoora Solar Observatory for the open data policy. We are thankful to Dr. P. Zlobec for helpful comments and suggestions. J.M. acknowledges a grant under MIUR Cofin.

Appendix

In the presented analysis we have used different approximations and assumptions. In Fig. 8 the density models used are shown. The two-fold Newkirk, two-, five-, and ten-fold Saito models are denoted in the legend of Fig. 8 as 2xNewk., 2xSaito, 5xSaito and 10xSaito.

The relationship between the downstream/upstream density jump X (compression) and the Alfvén Mach number M_A depends on the plasma-to-magnetic pressure ratio β and the angle θ between the shock normal and the upstream magnetic field. For the oblique shock the Alfvén Mach number M_A and the density jump X are related (taking for the adiabatic index $\gamma = 5/3$) as:

$$\left(M_{Ax}^2 - X\right)^2 \left[5\beta X + 2M_{Ax}^2 \cos^2\theta\,(X-4)\right] + M_{Ax}^2 X \sin^2\theta \left[(5+X)M_{Ax}^2 + 2X(X-4)\right] = 0. \quad (7)$$

Here $M_{Ax} = v/v_{Ax}$ is the Alfvén Mach number based on the $v_{Ax} = B_x/\sqrt{\mu\rho}$ component of the Alfvén velocity, where $B_x = B\cos\theta$ is the magnetic field component normal to the shock front (e.g., Mann et al. 1995). Since the sound speed and

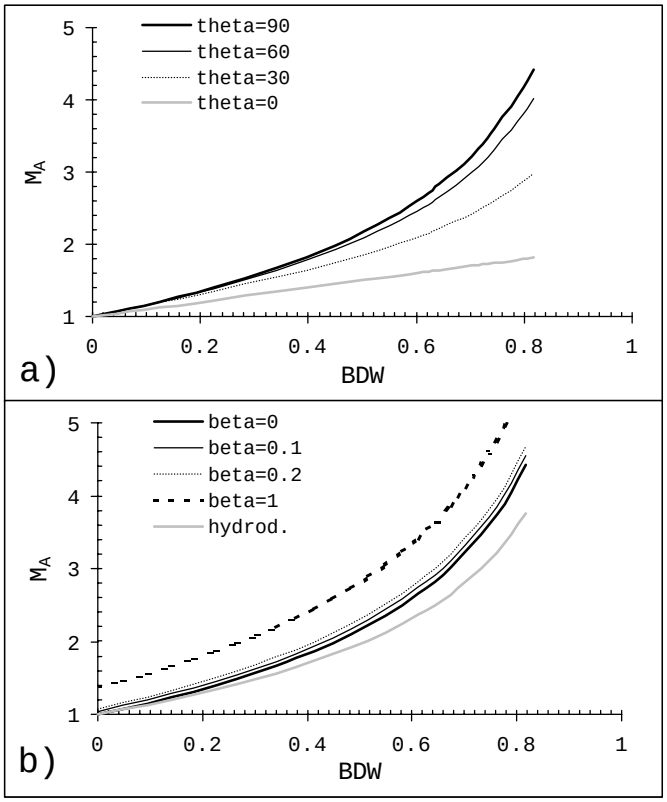

Fig. 9. Relationship between the Alfvén Mach number M_A and the relative band-split BDW obtained from $M_A(X)$ relationship by substituting $BDW = \sqrt{X-1}$ (see Eq. (2)). Results are presented for **a)** different angles θ between the shock normal and the magnetic field, with $\beta = 0$; **b)** different values of plasma-to-magnetic field pressure ratio β for the perpendicular shock, as well as for the hydrodynamic shock (gray line).

the Alfvén velocity are related as $c_s = v_A\sqrt{\gamma\beta/2}$ the sound Mach number can be also determined:

$$M_s = M_A\sqrt{\frac{2}{\gamma\beta}} = M_A\sqrt{\frac{1.2}{\beta}}. \quad (8)$$

In the case of the perpendicular shock ($\theta = 90^o$) Eq. (7) becomes:

$$M_A = \sqrt{\frac{X(X+5+5\beta)}{2(4-X)}}. \quad (9)$$

In the limiting case, for $\beta \to 0$ one finds:

$$M_A = \sqrt{\frac{X(X+5)}{2(4-X)}}. \quad (10)$$

On the other side, for $B \to 0$ (i.e. $\beta \to \infty$) one comes to the hydrodynamic approximation (sound shock wave), and the Mach number is:

$$M_s = \sqrt{\frac{3X}{4-X}}, \quad (11)$$

which was used by Smerd et al. (1974, 1975).

As Eqs. (7)–(11) show, the compression is limited to $X < 4$, corresponding to $f_U/f_L < 2$, i.e., $BDW < 1$, regardless on the value of β.

In the case of the longitudinal shock ($\theta = 0^o$):

$$M = \sqrt{X}, \quad (12)$$

but there is an upper limit on the compression which depends on the value of β:

$$X_{max} = 4 - \frac{5}{2}\beta \quad (13)$$

(Priest 1982).

The relationships given by Eqs. (7)–(12) are illustrated in Fig. 9 for different combinations of θ and β.

References

Aurass, H., Kurths, J., Mann, G., Chernov, G. P., & Karlický, M. 1987, Solar Phys., 108, 131
Bogod, V. M., Gelfreikh, G. B., Ryabov, B. I., & Hazifov, S. R. 1993, in The Magnetic and Velocity Fields of Solar Active Regions, ed. H. Zirin, G. Ai, & H. Wang, ASP Conf. Ser., 46, 302
Bougeret, J. L. 1985, in Collisionless Shocks in the Heliosphere, Geophys. Monograph 35 (AGU), 13
Bogod, V. M., Gelfreikh, G. B., Rybanov, B. I., & Hafizov, S. R. 1993, in The Magnetic and Velocity Fields of Solar Active Regions, ed. H. Zirin, G. Ai, & H. Wang, ASP Conf. Ser., 46, 302
Brosius, J. W., Davila, J. M., Thompson, W. T., et al. 1993, ApJ, 411, 410
Brosius, J. W., Davila, J. M., Thomas, R. J., & White, S. M. 1997, ApJ, 488, 488
Chae, J., Park, Y.-D., Moon, Y.-J, Wang, H., & Yun, H. S. 2002, ApJ, 567, L159
Cliver, E. W., Webb, D. F., & Howard, R. A. 1999, Sol. Phys., 187, 89
Dulk, G. A., & McLean, D. J. 1978, Sol. Phys., 57, 279
Dulk, G. A., Smerd, S. F., MacQueen, R. M., et al. 1976, Sol. Phys., 49, 369
Gary, G. A. 2001, Sol. Phys., 203, 71
Gergely, T. E., & Kundu, M. R. 1975, Sol. Phys., 41, 163
Gopalswamy, N., Thejappa, G., Sastry, Ch. V., & Tlamicha, A. 1986, Bull. Astron. Inst. Czech., 37, 115
Gopalswamy, N., Kaiser, M. L., Lepping, R. P., et al. 1998, J. Geophys. Res., 103, 307
Habbal, S. R., Woo, R., & Arnaud, J. 2001, ApJ, 558, 852
Kakinuma, T., & Swarup, G. 1962, ApJ, 136, 975
Klassen, A., Aurass, H., Klein, K.-L., Hofmann, A., & Mann, G. 1999, A&A, 343, 287
Klein, K.-L., Khan, J. I., Vilmer, N., Delouis, J.-M., & Aurass, H. 1999, A&A, 346, L53
Krüger, A., & Hildebrandt, J. 1993, in The Magnetic and Velocity Fields of Solar Active Regions, ed. H. Zirin, G. Ai, & H. Wang, ASP Conf. Ser., 46, 249
Ledenev, V. G., Tirsky, V. V., Tomozov, V. M., & Zlobec, P. 2002, A&A, submitted
Lin, H., Penn, M. J., & Tomczyk, S. 2000, ApJ, 541, L83
Magdalenić, J., & Vršnak, B. 2000, Hvar Obs. Bull., 24, 1
Mann, G., & Baumgärtl, K. 1988, ESA SP-285, 153
Mann, G., Classen, T., & Aurass, H. 1995, A&A, 295, 775
Mann, A., Aurass, H., Voigt, W., & Paschke, J. 1992, ESA SP-348, 129

Mann, G., Klassen, A., Classen, T., et al. 1996, A&AS, 119, 489
Mann, G., Aurass, H., Klassen, A., Estel, C., & Thompson, B. J. 1999, ESA SP-446, 477
Mann, G., Klassen, A., Aurass, H., & Classen, H.-T. 2002, A&A, submitted
Mollowo, L. 1988, Solar Phys., 116, 323
Nakariakov, V. M., & Ofman, L. 2001, A&A, 372, L53
Nelson, G. S., & Robinson, R. D. 1975, Proc. ASA, 2, 370
Nelson, G. S., & Melrose, D. B. 1985, in Solar radiophysics, ed. D. J. McLean, & N. R. Labrum (Cambridge Univ. Press, Cambridge), 333
Newkirk, G. Jr. 1961, ApJ, 133, 983
Patzold, M., Bird, M. K., Wolland, H., et al. 1987, Solar Phys., 109, 91
Prestage, N. P., Luckhurst, R. G., Paterson, B. R., Bevins, C. S., & Yuile, C. G. 1994, Solar Phys., 150, 393
Priest, E. R. 1982, Solar Magnetohydrodynamics (Reidel, Dordrecht)
Ramaty, R., & Petrosian, V. 1972, ApJ, 178, 241
Saito, K. 1970, Ann. Tokyo Astr. Obs., 12, 53
Smerd, S. F., Sheridan, K. V., & Stewart, R. T. 1974, in IAU Symp. 57, ed. G. A. Newkirk, 389
Smerd, S. F., Sheridan, K. V., & Stewart, R. T. 1975, ApL, 16, 23
Stewart, R. T. 1976, Solar Phys., 50, 437
Vršnak, B., & Lulić, S. 2000, Sol. Phys., 196, 157
Vršnak, B., Magdalenić, J., & Aurass, H. 2001a, Solar Phys., 202, 319
Vršnak, B., Aurass, H., Magdalenić, J., & Gopalswamy, N. 2001b, A&A, 377, 321
Yu, X.-F., & Yao, J.-X. 2002, Adv. Space. Res., 29, 469